Absolute absorption coefficient of $Cd_{1-x}Mn_xTe$ (x=0.09, 0.16, 0.34) near the E_0 gap in external magnetic fields

1990 J. Phys.: Condens. Matter 2 8669

(http://iopscience.iop.org/0953-8984/2/43/011)

J. Phys.: Condens. Matter 2 (1990) 8669–8679. Printed in the UK

Absolute absorption coefficient of $Cd_{1-x}Mn_xTe$ ($x = 0.09$, 0.16, 0.34) near the E_0 gap in external magnetic fields

W Limmer†, S Bauer†, H Leiderer†, W Gebhardt† and R N Bicknell-Tassius‡

† Institut für Festkörperphysik, Universität Regensburg, Universitätsstrasse 31, D-8400 Regensburg, Federal Republic of Germany

‡ Physikalisches Institut, Universität Würzburg, Am Hubland, D-8700 Würzburg, Federal Republic of Germany

Received 5 June 1990

Abstract. The optical absorption coefficient of $Cd_{1-x}Mn_xTe$ ($x = 0.09, 0.16, 0.34$) is determined near the E_0 gap at $T = 1\,K$ in external magnetic fields up to 5 T. Single-crystal $Cd_{1-x}Mn_xTe$ layers with thicknesses 1–2 μm were grown on a (001) GaAs substrate by MBE. The substrate was removed by mechanical polishing and chemical etching. In $Cd_{1-x}Mn_xTe$ a large splitting of the twofold degenerate Γ_6 conduction band and the fourfold degenerate Γ_8 valence band occurs at low temperatures in external magnetic fields. As a consequence the free exciton ground state splits into six components. In the Faraday configuration two allowed optical transitions for both right- and left-circular polarized light can be observed in the absorption spectrum. The measured splitting of the exciton ground-state energy as a function of the magnetic field is in good agreement with an existing theoretical band model for diluted magnetic semiconductors. Without an external magnetic field we obtain for the absorption coefficient a value of $4.0 \times 10^4\,cm^{-1}$ for the continuum exciton states near E_0.

1. Introduction

In the class of ternary II–VI compounds, known as diluted magnetic semiconductors (DMS) or semimagnetic semiconductors (SMSC), a part of the cations is randomly replaced by transition metal ions with permanent magnetic moments [1, 2]. The magnetic moments of Mn^{2+} ions in $Cd_{1-x}Mn_xTe$ arise from their $3d^5$ electrons, which give a total spin of $S = 5/2$. Without external magnetic fields DMS behave in a similar way to normal ternary semiconductors. This means that several crystal parameters, such as the lattice constant a_0 or the gap energy E_0, are x dependent and that due to the random distribution of Mn^{2+} ions in the crystal most properties of DMS can be described within the virtual crystal approximation [3]. $Cd_{1-x}Mn_xTe$ crystallizes in the zinc blende structure for Mn concentrations $0 \leq x \leq 0.77$ [4] and the fundamental energy gap varies from 1.6 eV for $x = 0$ to 2.7 eV for $x = 0.7$ at $T = 4\,K$ [5]. In the presence of external magnetic fields $\boldsymbol{B}$ the spin polarization of the Mn^{2+} ions leads to extremely large magneto-optical effects, such as giant Zeeman splitting of the excitonic band, large Faraday rotation or a giant Stokes shift in spin-flip Raman scattering [1]. These anomalously large effects have been explained by considering

0953-8984/90/438669+11$03.50

an exchange interaction between the localized $3d^5$ electrons of Mn^{2+} ions and band electrons [6].

The giant Zeeman splitting of the Γ_6 conduction and Γ_8 valence band near the centre of the Brillouin zone in external magnetic fields has been investigated by photoluminescence [7], reflectivity [8–10] and transmission [11,12] measurements. For the transmission technique, samples with a thickness below 1 μm are necessary since the absorption coefficient in the energy range of the exciton ground state is of the order of 10^5 cm^{-1}. Usually no absolute values have been given for the absorption coefficient α. This may be due to the inhomogeneous thickness and the large surface roughness of thin $Cd_{1-x}Mn_xTe$ samples, prepared from bulk crystals, which destroys any interference pattern of the transmitted light. However, these interference patterns are needed for the exact determination of the sample thickness and thus for the determination of α.

In this paper we present absolute values of the absorption coefficient α of MBE grown $Cd_{1-x}Mn_xTe$ layers near the free exciton ground state in the presence of external magnetic fields from $B = 0$ T to 5 T.

2. Theory

The exchange interaction between band electrons and localized $3d^5$ electrons of Mn^{2+} ions is usually described by a Heisenberg Hamiltonian [6,13–15]. In the molecular field approximation it can be written as

$$H_{ex} = -x\boldsymbol{\sigma} \cdot \langle \boldsymbol{S} \rangle \sum_{\boldsymbol{R}} J(\boldsymbol{r} - \boldsymbol{R}) \tag{1}$$

where x is the Mn concentration, $\boldsymbol{\sigma}$ the electron spin operator and $\langle \boldsymbol{S} \rangle$ the thermal average of the spin operators of the Mn^{2+} ions. J is the exchange interaction constant and the summation is carried out over all lattice sites $\boldsymbol{R}$. For $\boldsymbol{B} \parallel \hat{z}$ the thermal average $\langle \boldsymbol{S} \rangle$ can be replaced by its z component $\langle S_z \rangle$. This quantity is usually expressed by a Brillouin function B_S

$$\langle S_z \rangle = S_0 B_{5/2}\left(\frac{\frac{5}{2} g \mu_B B}{k_B (T + T_0)}\right) \tag{2}$$

where $g = 2$ and μ_B is the Bohr magneton. S_0 and T_0 are x-dependent parameters that take into account the fact that a fraction of Mn^{2+} ions form clusters of 2, 3 or more ions with strong antiferromagnetic ordering, producing no magnetic moment. In the presence of external magnetic fields the exchange interaction in equation (1) leads to a large splitting of the electron band states at the centre of the Brillouin zone. The energy spectra and the wavefunctions in Γ_6 conduction and Γ_8 valence bands can be calculated by means of the $\boldsymbol{k} \cdot \boldsymbol{p}$ method, neglecting Landau quantization and intrinsic spin splitting [9]. Figure 1 shows schematically the Zeeman-like splitting of the valence and conduction band states at the Γ-point of the Brillouin zone. Allowed optical transitions in the Faraday configuration ($\boldsymbol{B} \parallel \boldsymbol{k}_L$) for incident light with polarization vectors

$$\hat{e}_+ = \tfrac{1}{\sqrt{2}}(1, i, 0) \qquad \hat{e}_- = \tfrac{1}{\sqrt{2}}(1, -i, 0) \tag{3}$$

are indicated by full arrows. The corresponding transition energies E_i ($i = 1,\ldots,6$) and relative transition probabilities dw/dt are listed in table 1. The splitting parameters A and B are given by

$$A = -\tfrac{1}{6}xN_0\alpha\langle S_z\rangle \geq 0 \qquad B = -\tfrac{1}{6}xN_0\beta\langle S_z\rangle \leq 0 \tag{4}$$

where N_0 is the number of unit cells per unit volume and α and β are the exchange integrals for the conduction and valence bands, respectively. The products $N_0\alpha$ and $N_0\beta$ were determined experimentally to be [14]

$$N_0\alpha = 0.22\,\mathrm{eV} \qquad N_0\beta = -0.88\,\mathrm{eV}. \tag{5}$$

In the following an exciton will be assigned to each interband transition between exchange-split sub-bands of the Γ_6 conduction and the Γ_8 valence bands [9]. This means that we consider six different excitons, enumerated by 1–6 (see figure 1), each built up by a hole from one of the exchange-split valence sub-bands and an electron from one of the conduction sub-bands. In order to calculate the energies of the Zeeman split components of the free exciton ground state, the gap energy E_0 in table 1 has to be replaced by the exciton ground-state energy $E_{ex} = E_0 - Ry$ for $B = 0\,\mathrm{T}$. Ry denotes the exciton Rydberg energy with $Ry = 10.5\,\mathrm{meV}$ for CdTe.

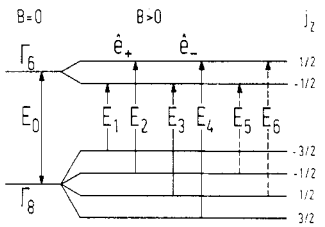

Figure 1. Schematic representation of the Zeeman-like splitting of Γ_6 conduction and Γ_8 valence band states at the Γ-point of the Brillouin zone in external magnetic fields. Allowed optical transitions in the Faraday configuration for left-($\hat{e}_-$) and right-circularly ($\hat{e}_+$) polarized incident light are indicated by full arrows.

Table 1. Allowed optical transitions between Γ_8 valence band states (v) and Γ_6 conduction band states (c) in the Faraday configuration (see figure 1). For both $\hat{e}_+$- and $\hat{e}_-$-polarized incident light two transitions are allowed with different relative transition probabilities dw/dt. The band splitting parameters A and B are defined in the text.

Transition	Transition energy	Polarization	dw/dt
$\lvert -\frac{3}{2}\rangle_v \rightarrow \lvert -\frac{1}{2}\rangle_c$	$E_1 = E_0 + 3B - 3A$	$\hat{e}_+$	3
$\lvert -\frac{1}{2}\rangle_v \rightarrow \lvert +\frac{1}{2}\rangle_c$	$E_2 = E_0 + B + 3A$	$\hat{e}_+$	1
$\lvert +\frac{1}{2}\rangle_v \rightarrow \lvert -\frac{1}{2}\rangle_c$	$E_3 = E_0 - B - 3A$	$\hat{e}_-$	1
$\lvert +\frac{3}{2}\rangle_v \rightarrow \lvert +\frac{1}{2}\rangle_c$	$E_4 = E_0 - 3B + 3A$	$\hat{e}_-$	3

3. Experimental details

Epitaxial growth of the $Cd_{1-x}Mn_xTe$ single layers were carried out in a four-chamber RIBER 2300 MBE system. The vacuum in the growth chamber was better than 6×10^{-10} Torr. Chemomechanically polished (001) GaAs wafers were employed as substrates for all growths. Prior to insertion into the MBE system the samples were degreased using standard solvents, etched in a (7:1:1) H_2SO_4:H_2O_2:H_2O solution and then rinsed in de-ionized water. Immediately prior to loading the substrates into the MBE system, they were briefly dipped in hydrochloric acid and rinsed in de-ionized water so as to remove any remaining surface oxide. The substrates were initially pre-heated for several minutes at 100 °C followed by a second preheat step at a higher temperature of 550–600 °C.

The substrate surface was monitored with reflection high-energy electron diffraction (RHEED) and x-ray photoelectron spectroscopy (XPS) to obtain the optimally clean and smooth surface.

The samples investigated in this paper have Mn concentrations of 9%, 16% and 34% and a thickness of 0.7 μm, 2.3 μm and 1.4 μm, respectively (see table 2). The gap energy of GaAs at $T = 4$ K ($E_0 = 1.52$ eV) is smaller than that of $Cd_{1-x}Mn_xTe$ ($E_0 \geq 1.60$ eV). Therefore, transmission measurements on $Cd_{1-x}Mn_xTe$ layers near E_0 can only be performed when the GaAs substrate is removed. In a first step the $Cd_{1-x}Mn_xTe$ layer was glued to a glass substrate and the GaAs substrate was mechanically polished down to a thickness of 100 μm. In a second step we removed the remaining substrate by chemical etching using a (100:1) H_2O_2 (30%) : NH_4OH (58%) solution. Finally the glue was dissolved in acetone and the $Cd_{1-x}Mn_xTe$ layer was loosely fixed on another glass substrate (see figure 2). In this way strain, induced by the different thermal expansion coefficients of layer and sample holder material, could be omitted.

Table 2. The average thickness d and the surface roughness Δd of the investigated samples were determined from the transmission spectra below the fundamental band gap. The absolute values of the absorption coefficient α at the exciton ground-state energy E_{ex} have been obtained by using equation (8).

$Cd_{1-x}Mn_xTe$	$x = 0.09$	$x = 0.16$	$x = 0.34$
d [μm]	0.7 ± 0.05	2.3 ± 0.03	1.4 ± 0.03
Δd [nm]	17 ± 5	22 ± 5	29 ± 5
E_{ex} [eV] ($T = 1$ K)	1.739 ± 0.002	1.856 ± 0.005	2.145 ± 0.003
$\alpha(E_{ex})$ [10^4cm^{-1}]	4.6±0.3	—	4.4±0.2
$\alpha(E_0)$ [10^4cm^{-1}]	4.0±0.3	—	4.2±0.2

The $Cd_{1-x}Mn_xTe$ layers were inserted in a liquid-He bath cryostat ($T = 1$ K) within a superconducting BOC split-coil magnet system, which enabled us to apply external magnetic fields up to 5 T. The transmission measurements were performed in the Faraday configuration with the direction of the incident light perpendicular to the (001) surface of the layer. As a light source we used a halogen lamp with an integral intensity less than 1 mW. Left- ($\hat{e}_-$) or right-circularly ($\hat{e}_+$) polarized light was produced by a linear polarizer followed by an achromatic quarter-wave plate. The incident light was focused onto the sample using achromatic lenses. The detection system was computer controlled and consisted of a Jarrel–Ash 1m double-grating monochromator with a RCA 31034 GaAs photomultiplier tube connected to the computer system.

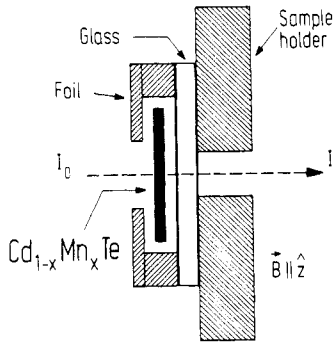

Figure 2. The self-supporting $Cd_{1-x}Mn_xTe$ layers were loosely fixed to the sample holder in order to avoid strain, induced by the different thermal expansion coefficients.

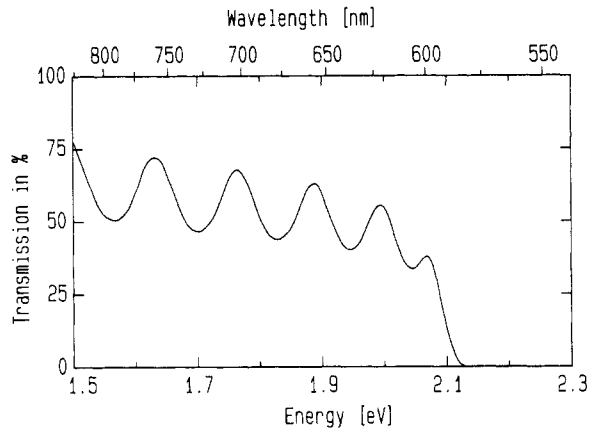

Figure 3. Transmission spectrum of $Cd_{0.66}Mn_{0.34}Te$ for $B = 0\,T$ at $T = 1\,K$. The thickness d of the layer can be determined from the interference pattern that appears for photon energies below the fundamental gap.

The thicknesses of the $Cd_{1-x}Mn_xTe$ layers were determined from the interference patterns of the transmission spectra which are observed for photon energies below the fundamental gap energy [16]. Figure 3 depicts a typical transmission spectrum of $Cd_{0.66}Mn_{0.34}Te$ for $B = 0\,T$. The interference pattern vanishes for photon energies near the band gap since the absorption coefficient increases very strongly. The average thickness d of the layer can be determined from the spectral position of the interference extrema using the relation

$$d = \frac{M\lambda_1\lambda_2}{2[n(\lambda_1)\lambda_2 - n(\lambda_2)\lambda_1]}. \tag{6}$$

Here λ_1 and λ_2 denote the wavelength positions of interference minima or maxima, $n(\lambda)$ is the wavelength-dependent refractive index and M is the number of oscillations between the minima or maxima at λ_1 and λ_2. The procedure that must be carried out in order to obtain the surface roughness Δd of the layer is much more complicated and can be found in [17]. The values of d, Δd for the investigated layers are listed in table 2. In the spectral range of strong absorption the interference fringes disappear. In

this case the measured transmission T is related to the absorption coefficient α by [16]

$$T = I/I_0 = \frac{16n^2 \exp(-\alpha d)}{(n+1)^4} \tag{7}$$

where I denotes the transmitted and I_0 the incident power. Thus, we obtain for the absorption coefficient

$$\alpha = -\frac{1}{d} \ln\left[\frac{(n+1)^4}{16n^2} T\right]. \tag{8}$$

4. Results and discussion

Figure 4 depicts the absolute absorption coefficient α of $Cd_{0.91}Mn_{0.09}Te$ at $T = 1\,K$ for the magnetic fields $B = 0\,T$ and $B = 4\,T$. For $B = 0\,T$ one absorption maximum appears at the exciton ground-state energy $E_{ex} = 1.739\,eV$ with $\alpha = 4.6 \times 10^4\,cm^{-1}$ (see table 2). For the continuum exciton states near E_0 we obtain $\alpha = 4.0 \times 10^4\,cm^{-1}$. With increasing magnetic field the absorption maximum splits into a weak and a strong absorption line for both $\hat{e}_+$- and $\hat{e}_-$-polarized incident light. For $\hat{e}_+$-polarized light the strong line is shifted 45 meV to lower energies while in the weak structure there is almost no change of its position. In the case of $\hat{e}_-$-polarized light the strong line is shifted 45 meV to higher energies, and again the weak structure is only slightly shifted. In figure 5 absorption spectra of $Cd_{0.91}Mn_{0.09}Te$ are displayed for magnetic fields from $B = 0\,T$ to $B = 5\,T$. The absorption spectra are separated vertically from each other in order to give an overview of the experimental results. They are plotted on the same scale and the corresponding absolute values are easily deduced from a comparison with figure 4.

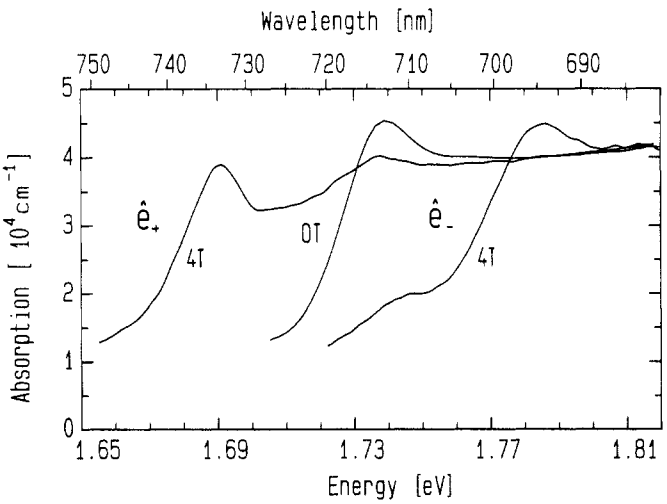

Figure 4. Absolute absorption coefficient α of $Cd_{0.91}Mn_{0.09}Te$ at $B = 0\,T$ and $B = 4\,T$ for right- ($\hat{e}_+$) and left-circularly ($\hat{e}_-$) polarized incident light.

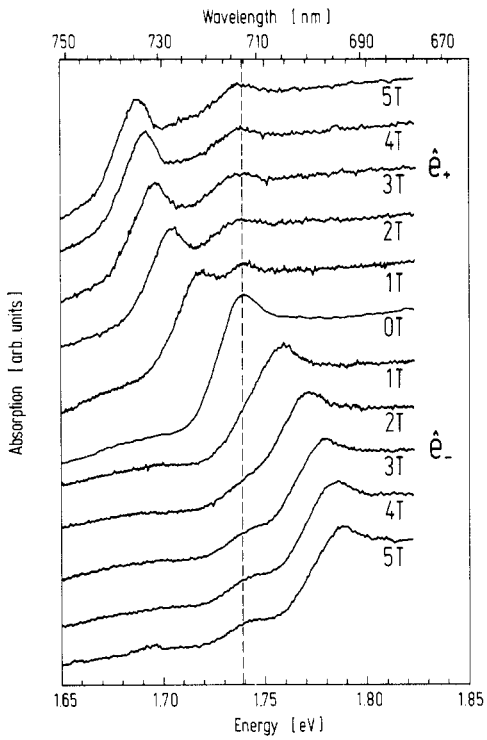

Figure 5. Absorption spectra of $Cd_{0.91}Mn_{0.09}Te$ for $B = 0$ T to 5 T with $\hat{e}_+$- and $\hat{e}_-$-polarized incident light. The spectra have been shifted vertically to each other for clarity.

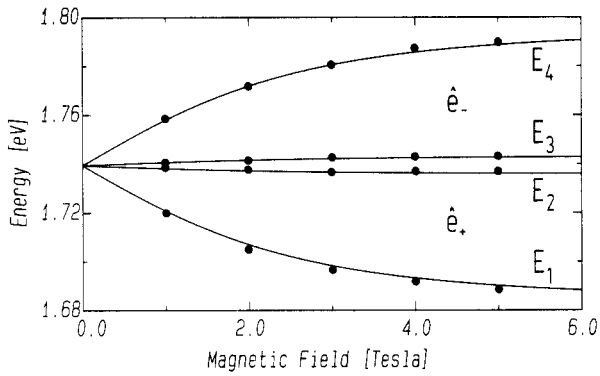

Figure 6. The absorption peaks of figure 5 (full circles) plotted as a function of the external magnetic field. The full curves are numerical calculations for the exciton ground-state energies E_{ex} of excitons 1–4.

It can clearly be seen that the strong absorption line is shifted with increasing magnetic field while the weak structure almost maintains its position. In figure 6 the positions of the absorption peaks are plotted as a function of the magnetic field (full circles). The splitting of the absorption lines increases linearly at low fields and tends to saturate at higher field values. The full curves represent the calculated ground-state energies of the four excitons 1,...,4 which were introduced in section 2. The calcula-

tions were performed using equations (2), (4) and (5), and the transition energies E_i (i = 1,...,4) from table 1 where the gap energy E_0 has been replaced by the exciton ground-state energy E_{ex}. The parameters S_0 and T_0 were taken from [14] and are listed in table 3. Figure 6 clearly demonstrates that the four exciton ground-state energies exhibit the same energy shift in magnetic fields as the corresponding interband transition energies E_i between the Zeeman-split Γ_6 conduction and Γ_8 valence sub-bands in the one-electron model (see figure 1). The different strengths of the absorption lines from excitons 1,4 and excitons 2,3 are in agreement with the different relative transition probabilities dw/dt listed in table 1. For the excitons 1,4 the transition probabilities are three times larger than those for the excitons 2, 3 and thus the absorption peaks are more pronounced.

Table 3. The x dependent empirical parameters S_0 and T_0 enter into the Brillouin function of equation (2). The values for $x \leq 0.30$ were taken from [14] and those for $x = 0.34$ were obtained by extrapolation.

x	0.09	0.16	0.34
S_0	1.14	0.82	0.46
T_0	3.6	5.7	22.5

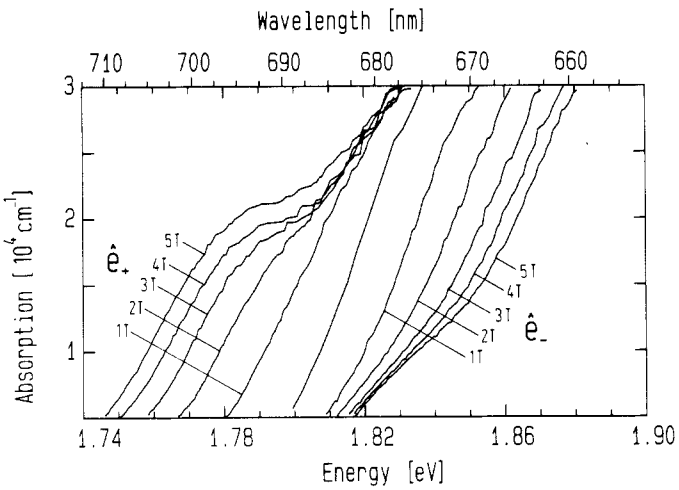

Figure 7. Absorption spectra of $Cd_{0.84}Mn_{0.16}Te$ for $B = 0\,T$ to $5\,T$ with $\hat{e}_+$- and $\hat{e}_-$-polarized incident light. Because of the large layer thickness $d = 2.3\,\mu m$ no transmitted light could be detected for $\alpha \geq 3 \times 10^4\,cm^{-1}$.

The absorption spectra of $Cd_{0.84}Mn_{0.16}Te$ and $Cd_{0.66}Mn_{0.34}Te$ are shown in figure 7 and figure 9, respectively. In the case of $Cd_{0.84}Mn_{0.16}Te$ the averaged sample thickness $d = 2.3\ \mu m$ is much larger than that for $Cd_{0.91}Mn_{0.09}Te$ (see table 2) and therefore the transmission signals could not be discerned from the background for $\alpha \geq 3 \times 10^4\,cm^{-1}$. However, the shift of the strong absorption peaks (excitons 1 and 4) can be determined from figure 7. Together with the exciton ground-state energy $E_{ex} = 1.856\,eV$ of $Cd_{0.84}Mn_{0.16}Te$ we obtain the positions for the (1s) states of excitons 1 and 4 as shown in figure 8. They are in good agreement with the calculated

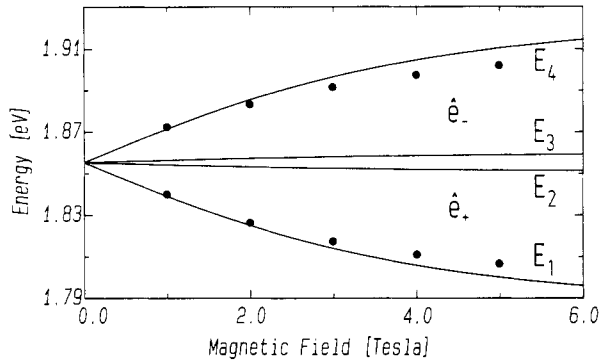

Figure 8. Energetic position of the exciton ground-state energies of $Cd_{0.84}Mn_{0.16}Te$ for excitons 1 and 4; experiment (•) and theory (—).

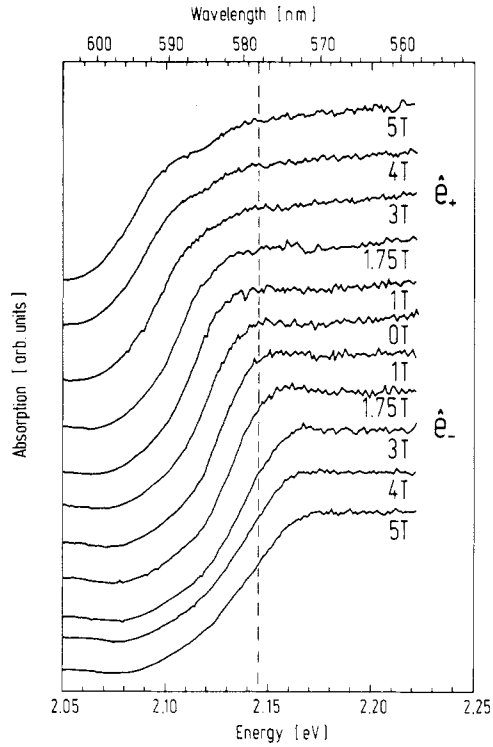

Figure 9. Absorption spectra of $Cd_{0.66}Mn_{0.34}Te$ for $B = 0\,T$ to $5\,T$ with $\hat{e}_+$- and $\hat{e}_-$-polarized incident light.

energies using the parameters S_0 and T_0 from table 3. Figure 9 displays the absorption spectra of $Cd_{0.66}Mn_{0.34}Te$ for $B = 0\,T$ to $B = 5\,T$. The absorption structures are less pronounced than in the case of $Cd_{0.91}Mn_{0.09}Te$. This may be due to a larger inhomogeneous alloy broadening induced by the higher Mn concentration. While the weak absorption structures (excitons 2 and 3) can hardly be localized in the spectra, the strong absorption peaks are still detectable and their positions are plotted in figure 10 as a function of the applied magnetic field. Although the empirical parameters S_0

and T_0 for $Cd_{0.66}Mn_{0.34}Te$ had to be extrapolated from the values given in [14] the agreement of theory and experiment is still satisfying.

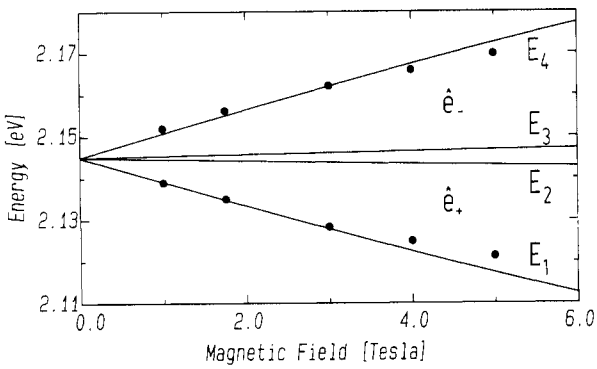

Figure 10. Energetic position of the exciton ground-state energies of $Cd_{0.66}Mn_{0.34}Te$ for excitons 1 and 4; experiment (•) and theory (—).

5. Conclusion

The absolute absorption coefficient α of MBE grown $Cd_{1-x}Mn_xTe$ (x = 0.09, 0.16, 0.34) layers has been measured near the fundamental absorption edge at $T = 1\,K$ for external magnetic fields from $B = 0\,T$ to $5\,T$. For zero magnetic field typical values of the absorption coefficient are $\alpha = 4.5 \times 10^4\,cm^{-1}$ at the lowest discrete exciton energy E_{ex} and $\alpha = 4.0 \times 10^4\,cm^{-1}$ for the continuous exciton energies near E_0. In the Faraday configuration the exciton ground-state absorption line splits into four components in the presence of external magnetic fields. Two lines appear for right- and two for left-circularly polarized light. This field-dependent Zeeman-like splitting is in good agreement with theoretical calculations considering the influence of the exchange interaction between band electrons and localized magnetic moments on the Γ_6 conduction and Γ_8 valence bands.

References

[1] Brandt N B and Moshchalkov V V 1984 *Adv. Phys.* **33** 193
[2] Furdyna J K 1982 *J. Appl. Phys.* **53** 7637
[3] Chadi D J and Cohen M L 1973 *Phys. Rev.* B **7** 692
[4] Giriat W and Furdyna J K 1988 *Semiconductors and Semimetals* vol 25, ed R K Willardson and A C Beer (London: Academic) p 1
[5] Bücker R, Gumlich H E and Krause M 1985 *J. Phys. C : Solid State Phys.* **18** 661
[6] Gaj J A 1988 *Semiconductors and Semimetals* vol 25, ed R K Willardson and A C Beer (London: Academic) p 275
[7] Ryabchenko S M, Terletskii O V, Mizetskaya I B and Oleinik G S 1981 *Fiz. Tekh. Poluprov.* **15** 2314 (Engl. Transl: 1981 *Sov. Phys.-Semicond.* **15** 1345)
[8] Komorov A V, Ryabchenko S M, Terletskii O V, Zheru I I and Ivanchuk R D 1977 *Zh. Eksp. Teor. Fiz.* **73** 608 (Engl. Transl: 1977 *Sov. Phys.-JETP* **46** 318)
[9] Gaj J A, Ginter J and Galazka R R 1978 *Phys. Status Solidi* b **89** 655
[10] Rebman G, Rigaux C, Bastard G, Menant M, Triboulet R and Giriat W 1983 *Physica* B **117**, B **118** 452

[11] Twardowski A, Nawrocki M and Ginter J 1979 *Phys. Status Solidi* b **96** 497
[12] Nguyen The Khoi, Ginter J and Twardowski A 1983 *Phys. Status Solidi* b **117** 67
[13] Bastard G, Rigaux C, Guldner Y, Mycielski J and Mycielski A 1978 *J. Physique* **39** 87
[14] Gaj J A, Planel R and Fishman G 1979 *Solid State Commun.* **29** 435
[15] Galazka R R and Kossut J 1980 *Narrow Gap Semiconductors: Physics and Applications (Lecture Notes in Physics Series 133)* (Berlin: Springer) p 245
[16] Swanepoel R 1983 *J. Phys. E: Sci. Instrum.* **16** 1214
[17] Swanepoel R 1984 *J. Phys. E: Sci. Instrum.* **17** 897